applied sciences

MDPI

Article

Optimal Wavelet Selection for DC Fault Detection in Multi-Terminal VSC-HVDC Grids: A Performance Comparison with HIL Validation

Akash Sovis [1], Manilka Jayasooriya [1,*], Muhammad Naveed Iqbal [1], Kamran Daniel [2], Hadi Ashraf Raja [2], Rana Arslan Qadar [2] and Noman Shabbir [2,3,*]

[1] Department of Engineering, University of Staffordshire, Stoke-on-Trent ST4 2DE, UK; akash.sovis@staffs.ac.uk (A.S.); naveed.iqbal@staffs.ac.uk (M.N.I.)
[2] Department of Electrical Power Engineering and Mechatronics, Tallinn University of Technology, 19086 Tallinn, Estonia; kamran.daniel@taltech.ee (K.D.); hadi.raja@taltech.ee (H.A.R.); rana.qadar@taltech.ee (R.A.Q.)
[3] FinEst Centre for Smart Cities, Tallinn University of Technology, 19086 Tallinn, Estonia
* Correspondence: manilka.jayasooriya@staffs.ac.uk (M.J.); noman.shabbir@taltech.ee (N.S.)

Abstract

Rapid and reliable DC fault detection is critical to the safe operation of Voltage Source Converter High Voltage Direct Current (VSC-HVDC) multi-terminal grids, where low system impedance causes fault currents to rise within milliseconds, demanding detection within 1 ms. Discrete Wavelet Transform (DWT) has emerged as a leading signal processing technique for this purpose. However, no comprehensive performance study exists comparing the principal mother wavelets Daubechies (db), Symlets (sym), and Coiflets (coif) across the key operational variables of noise environment, cable length, and grid topology. This paper presents a systematic comparative evaluation of six wavelets (db4, db8, sym3, sym5, coif3, coif5) for DC fault detection in both three-terminal and four-terminal VSC-HVDC grids, assessing performance against four metrics: detection delay, accuracy, noise tolerance, and computational efficiency. Internal close-up and internal remote DC faults were simulated under no-noise conditions and white Gaussian noise levels of 30 dB, 20 dB, and 10 dB, with additional tests at cable lengths of 50 km and 400 km. Results demonstrate that db4 consistently achieves the lowest detection delay with high accuracy for four-terminal configurations under varying noise conditions, while sym3 proves most adaptable across both topologies for multiple cable lengths owing to its consistent detection delay. Real-time validation using an OPAL-RT hardware-in-the-loop (HIL) platform confirms the simulation findings, reinforcing the suitability of sym3 for multi-terminal grid deployment. These results provide actionable guidance for the selection of mother wavelets in DWT-based protection algorithms for modern VSC-HVDC systems.

Keywords: HVDC fault detection; wavelet comparison; hardware-in-the-loop validation

Academic Editor: Roberto Zivieri

Received: 28 April 2026
Revised: 16 May 2026
Accepted: 19 May 2026
Published: 22 May 2026

1. Introduction

With the growing energy demand and the need for decarbonisation, a high level of renewable energy (RE) penetration is expected with 51% of the total generation mix to be from RE sources by 2040 [1]. To accommodate the high penetration of RE a continuous network infrastructure development is needed to maintain quality energy generation, and as most of the RE is located in remote areas, efficient bulk power transmission is

crucial [2,3]. Energy transmission can be achieved via either HVAC or HVDC links, as mentioned previously. AC was preferred until Dr. Uno Lamm introduced the idea of placing grading electrodes in the gap of the mercury valve, which, at the time, was not economically feasible, as mercury arc valves were not capable of withstand high voltage (HV); the introduction proposed by Dr. Uno Lamm proved to significantly improve the voltage distribution and withstanding capabilities. This led to experimental plants in Sweden and the USA to investigate the use of mercury arc valves in transmission systems and later to the first commercial HVDC system built in 1954 in Sweden [4,5]. Later, silicon-controlled rectifiers were discovered (which is now known as thyristor) to achieve very important characteristics such as the HV blocking state in both the forward and reverse state, low voltage conduction state, and the ability to remain in conduction until the current dropped to zero, and finally, it conducted in both directions when it failed. Further development of this technology led to mercury arc valves being replaced by thyristor valves, which offered better efficiency, power density, and flexibility [6,7].

Although HVAC has dominated as the preferred method for transmission due to the increased size of the system and the increased losses over a large distance, it has lost its edge against HVDC, which is now the preferred method of power transmission with several projects underway, such as the Nord-Link in Europe, interconnecting Germany and Norway, spanning over 623 km. Such connections help stabilise the grid, such as where Germany can import hydropower during peak hours and transfer solar and wind to Norway during surplus [8]. Over the years, several major HVDC projects have been completed, such as China's Xianjiba-Shanghai, a 6400 MW 500 kV link over 1891 km, and Brazil's Itaipu HVDC link connecting hydroelectric generators to Sao Paulo, transmitting 6300 MW at 600 kV over 800 km [9,10].

HVDC offers several advantages over HVAC. HVDC has greater power per conductor and no skin effect, the line does not require reactive compensation, and asynchronous interconnection is possible [11,12]. However, the substations required for HVDC to function are very expensive, need reactive power, and require filters to mitigate harmonics. Although HVDC has a higher initial cost as it requires expensive rectifiers and inverters, over longer distances, they are found to be more economical as the breakeven point is about 800 km for overhead lines and 50 km for undersea cables [11]. Additionally, HVDC only requires one or two cables, depending on the connection, against the three used in HVAC; modern cables have been designed to have a higher power density, making it more viable than HVAC [13–15].

Moreover, existing HVAC lines can be refurbished and reused for a larger transmission capacity, making the environmental impact of HVDC very low. A feasibility study of converting a 380 kV AC line to a hybrid AC/DC operation was found to double the power capacity in the converted DC circuit [16–19].

1.1. LCC vs VSC Systems Overview

The process of HVDC systems lies in the conversion of current from AC to DC before transmission and DC to AC at the receiving end. Converters are crucial elements that enable this transmission, where rectifiers are needed to convert AC to DC and inverters to convert from DC to AC; currently, there are two ways to achieve this conversion: either using thyristors or by using IGBTs. A converter using a thyristor is called a line commutated converter (LCC); a thyristor is a switch in which the turn-on is controlled by a gate pulse, and the turn-off naturally occurs during the zero crossing of the AC supply [20,21]. Due to the high surge current endurance and higher efficiency, LCCs have been widely used since the 1960s for the transmission of high power with projects such as Zhundong-Sichuan in China, which transmits 10,000 MW at 1100 kV over 2600 km, and Longdong-Shandong,

a 926 km overhead line transmitting 8000 MW [22,23]. However, LCCs cannot black start due to the lack of frequencies. When a blackout occurs, the LCCs consume a high amount of reactive power and need capacitor banks to compensate for the reactive power absorbed by the converter; moreover, it is very susceptible to commutation failure during inverter AC faults and need fast circuit breakers [24–26]. To mitigate this issue, capacitor commutated converters have been developed; they use commutation capacitors in series with the converter transformer and the thyristor valves, allowing better commutation failure performance when connected to weak networks [20,21]. A single-line diagram of an LCC HVDC topology is shown in Figure 1.

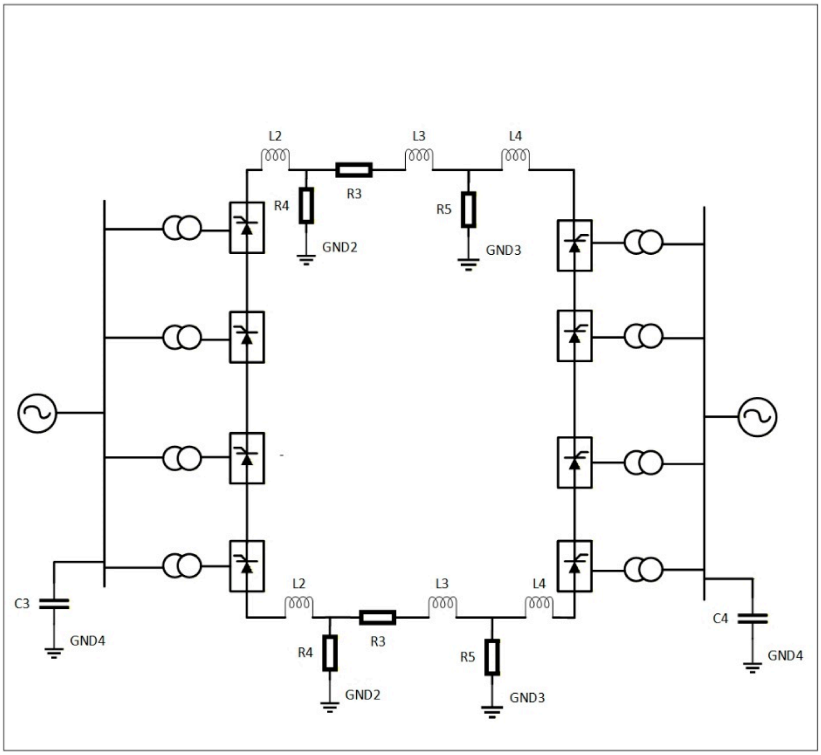

Figure 1. Single-line diagram of an LCC HVDC system.

Later in the 1990s, when semiconductors such as the insulated gate bipolar transistor (IGBT) in which both the turn on and turn off could be controlled, were developed, a new HVDC system based on a voltage source converter (VSC) emerged. This new system has considerable advantages such as the independent control of active and reactive power and black start capability, as the inverter side can create its own AC voltage by switching the bridges on and off rapidly [27,28]. They do not experience commutation failures, although they are more vulnerable to DC faults, as DC systems have low inductances and the fault current can increase rapidly [29,30]. Moreover, VSC can use advanced switching techniques such as the pulse width modulator (PWM) to operate in lower switching frequencies, decreasing the harmonic filter sizing and leading to a significant reduction in reactive power equipment compared to LCC [2,31,32].

However, as shown in [22], IGBTs have lower ratings than thyristors, with a maximum voltage rating of 1700 V against the 8000 V of the thyristor. This also translates into the amount of power that the VSC-based system can transmit, as shown in one of the largest VSC HVDC projects, the Zhangbei grid interconnecting Beijing, Fengning, and Kangbao, with a maximum transmission power of 3000 MW and operating at 500 kV [32,33].

The basic structure of the VSC stations employed in existing links are two level arrangements, utilising a series/parallel string of IGBT valves, with a structure like the thyristor-based six-pulse converter [29,34]. This topology enables clamping two voltage

levels to the AC terminal of the converter; however, a PWM needs to be used to approximate the desired voltage, creating unwanted distortion, which requires filtering [35]. To mitigate this disadvantage, a new topology, 'modular multilevel converter' (MMC), was developed; this topology depends on the basic cell structure of two terminal switching and a DC storage capacitor, forming a submodule. A number of chosen submodules forms the converter, each providing one step in the resulting AC waveform and allowing it to scale the topology to any voltage level by using the right number of submodules. This new topology offers several advantages, such as the arm current can flow continuously, it can be controlled to give a desired value, it eliminates the requirements for filters from the DC bus, and the DC bus voltage is now controlled by the converter's control system [36–40]. Notable projects include Chongqing-Hubei in China, which was commissioned in 2018 to transport 2500 MW at 420 kV, and the North Sea Link in the UK, commissioned by ABB in 2021 to transmit 1400 MW at 525 kV [39]. A VSC HVDC system is shown in Figure 2.

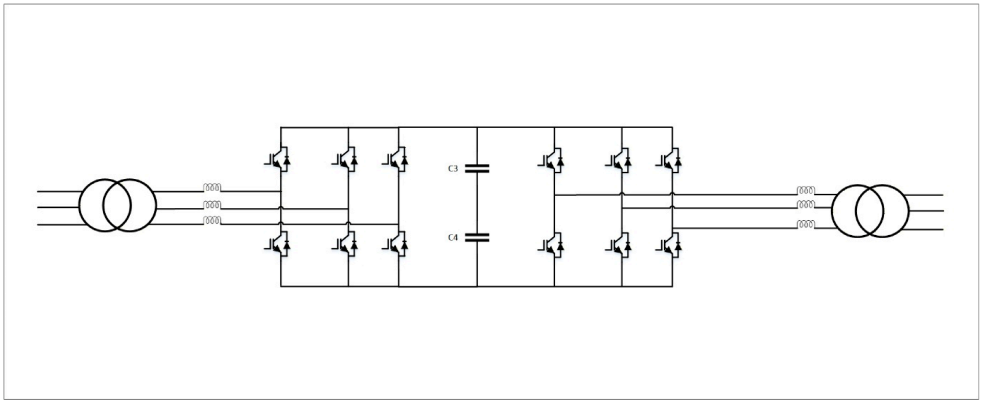

Figure 2. VSC HVDC system.

1.2. System Configuration

Depending on the purpose and location of the converter stations, there are various configurations to choose from, such as back-to-back, monopolar, bipolar, homopolar, and multiterminal. The back-to-back interconnection is the simplest of them. It consists of connecting two converters that are close to each other and can be connected without any long transmission lines. This configuration is used mainly to connect two asynchronous links with two systems with different frequencies, and due to the lack of transmission lines, the DC transmission losses in this system are very low [41].

The monopolar interconnection involves two converters connected by a single conductor for power transmission, and the ground acts as the return path for the current. When operating in this configuration, the one conductor carries the nominal voltage, and the return path carries zero to low voltage [42]. Although this is the more economical configuration, by using the sea or earth as the return path, it causes environmental concerns due to the ground current, and the corrosion of metal objects buried in the ground can affect water chemistry [43].

The bipolar configuration, the most popular configuration, uses two independent poles, one negative and the other one positive, to transmit the power. During fault times in one of the poles, the other pole can function using the ground as the return path (monopolar configuration) and still carry 50% of the total capacity [39,44,45]. The homopolar configuration consists of two or more conductors with the same polarity (either positive or negative), with the midpoint of the inverter being used at the ground return path. This configuration is economical but less reliable, as power outages can happen if either line experiences faults.

Finally, the multi-terminal configurations involve interconnecting more than two converter stations in different areas through a common DC network. This configuration

allows for renewable energy integration; it allows for power flow between any pair of terminals. However, the main drawbacks include the increased control complexity and the hardship in DC fault isolation [46].

The model used for these studies was built on MATLAB 2025a SIMULINK, based on a standard multiterminal HVDC grid design comprising 4 AC terminals, each connected to a bidirectional VSC converter for AC-to-DC conversion. The system can be said to be formed by connecting two two-terminal grids, each connected by 200 km DC cables. Interconnecting the grid between the rectifier and inverter is a 200 km pi-section DC cable. Furthermore, a 100 kΩ DC load is also introduced, connected to the grid via 45 km cables to test external faults, which will then be used as the threshold to distinguish between internal and external faults in the protection algorithm. Additionally, this DC load also doubles as the third terminal in the three-terminal system.

Finally, DC capacitors, harmonic filter, and smoothing reactors are used to reduce distortions that could arise from HVDC conversion and resonance. The smoothing reactors are installed to minimise the DC current, with 0.1 H inductors on each side of the transmission line. This model was chosen to match the already existing models to solely focus on the fault detection algorithm and provide a comprehensive benchmark study on the wavelets themselves, removing the differences that may occur with a different model. The design specifications of the model used are recorded in Table 1.

Table 1. System configuration.

Component	Sending End Terminal (1, 3)	Receiving End Terminal (2, 4)
AC Voltage Source	230 kV, 50 Hz, L = 62.23 mH, R = 13.79 Ω, Lp = 31.02 mH	230 kV, 50 Hz, L = 62.23 mH, R = 13.79 Ω, Lp = 31.02 mH
Transformer	200 MVA, 230/100 kV, 50 Hz wye-grounded/Delta	200 MVA, 100/230 kV, 50 Hz wye-grounded/Delta
Phase Reactor	R = 0.075 Ω, L = 0.023 H	R = 0.075 Ω, L = 0.023 H
VSC	Rectifier: 3-phase 6 pulse IGBT/diode, Rs = 5000 Ω, Cs = 1 μF, Ron = 1 mΩ	Inverter: 3-phase 6 pulse IGBT/diode, Rs = 5000 Ω, Cs = 1 μF, Ron = 1 mΩ
DC Capacitor Bank	2 × 70 μF, 2 × 12 μF	2 × 70 μF, 2 × 12 μF
Smoothing Reactor	Rs = 25.1 mΩ, 8 mΩ each	Rs = 25.1 mΩ, 8 mΩ each
DC Transmission Line	4 × 200 km R = 13.9 mΩ L = 0.159 mH C = 0.231 μF Ls = 4 × 0.1 H	4 × 200 km R = 13.9 mΩ L = 0.159 mH C = 0.231 μF Ls = 4 × 0.1 H

1.3. Faults in HVDC Systems

The main barrier against the mass implementation of HVDC systems is the lack of robust fault protection systems. Faults occurring in HVDC systems can be categorised into AC faults, internal converter faults, and DC faults. These faults are usually caused by isolation failures due to short circuits, switching, and lighting events [47–49]. AC faults can be classified as either symmetrical or asymmetrical faults; symmetrical faults include a three-phase short circuit and three phase voltage sag/swell, whereas asymmetric faults include line to line faults, line to ground faults, and double line to ground faults. When such faults happen in LCCs, it leads to commutation failures, leading to DC voltage collapse. Internal converter failures include overvoltage and overcurrent, which are due to the

sudden increase in the load or to a fault current increase due to AC or DC faults. Additional converter faults can occur due to the failure of power electronics devices [17,50,51].

Finally, the most frequent faults are the ones incurred on the DC side; there are two main types of faults that can occur: DC line-to-line fault and DC line-to-ground fault. Line-to-line faults are rarer but more severe, as the IGBTs will be blocked to avoid them being exposed to overcurrent. This fault can be divided into three stages:

Capacitor Discharge Stage—In this stage, a loop circuit without a source is formed, and the DC capacitors react to it by discharging through a cable impedance.

Diode Freewheeling Stage—As the capacitor voltage is now zero, the freewheeling diodes connected in anti-parallel with the semiconductor devices, to protect them from overvoltage, start conducting, driven by the line inductance. At this stage, there is a huge amount of current going through the diodes, which can lead to damage. Then, the DC current will reduce rapidly.

Capacitor Recharging Stage—In this last stage, the DC link capacitor, cable inductance, and AC side form a forced response, and the capacitor will start charging [51–54]. A line-to-ground fault is a more likely scenario, as potential faults can occur from cable aging or other physical damage. This fault will produce ground points beside the midpoint of the DC link capacitor, and the neutral ground link of the transformer. This fault can be divided into three stages: [55–58].

DC-Side Capacitor Discharge Stage—A discharge circuit is formed among the fault pole capacitor and the fault impedance through the fault line. After the fault occurred, the system started experiencing discharge in the DC capacitor.

Grid-Side Current Feeding Stage—With the DC side capacitor discharging, the DC voltage drops constantly. When this DC voltage drops to below any grid phase voltage, the system will experience the grid side current feeding stage. During this stage, a current circuit is established between the neutral ground link of the transformer and the grounding point of the fault line through the freewheeling diodes. This grid-side current will flow to the DC side through this circuit. This is the stage where the DC side capacitor is charged through the fault line by the AC power. If good control is implemented, the DC voltage can be kept above the AC phase voltage, and this stage is skipped [59].

Voltage Recovery Stage—This stage occurs when the fault pole capacitor voltage drops, and the non-fault pole capacitor voltage rises with the capacitor discharging, gradually restoring the DC voltage. A classification diagram of HVDC transmission line faults is shown in Figure 3.

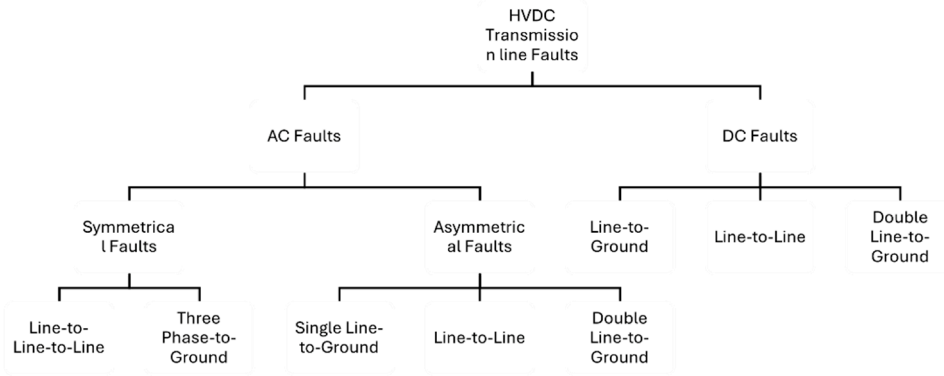

Figure 3. HVDC transmission line fault classification.

1.4. Fault Detection

From what has been discussed thus far, HVDC systems require fast fault detection systems to identify and prevent the converters. When a fault occurs, the DC circuit breaker should clear the fault within 5 ms due to the low impedance of the DC system, requiring

the fault to be detected under 1 ms by the protection algorithm (including any delays in the hardware in loop) [55,56]. The general requirements that a fault protection system should have are as follows [57–61]:

Selectivity: the protection algorithm should be able to accurately identify the faulty section. It should be able to distinguish between internal faults, where it needs to be tripped, and external faults, where it should not be tripped.

Speed: It should be able to detect the fault as soon as possible, giving the circuit breaker enough time to trip.

Sensitivity: the algorithm is sensitive to weak faults (faults with high resistance).

Security: the algorithm should not malfunction for an external fault, i.e., for faults that are outside the defined zone.

Generally, all protection techniques fall under two categories: either unit-based or non-unit-based. Non-unit-based techniques involve using algorithms that use information from the local terminal and do not need any communication channels. Unit-based techniques involve algorithms using information from local and remote terminals requiring communication channels, therefore incurring communication delays [60–67]. Furthermore, protection systems can be classified as either steady state (used in AC systems) or transient-based protection principles. Due to the fast nature of the faults incurred in HVDC systems, the faults need to be identified during the transient. Over the years, many signal processing techniques analysing current and voltage information using innovative mathematical techniques have emerged. These techniques can be categorised into time-domain, frequency domain, and time-frequency domain methods [68].

Time-domain techniques include empirical mode decomposition, intrinsic time decomposition, and mathematical morphology [69–71].

Frequency-domain techniques include the Fourier transform, discrete Fourier transform, and fast Fourier transform [72].

Time-frequency techniques include different variants of wavelet transform, Stockwell transform, short-time Fourier transform, Hilbert Huang transform, etc. [73–75].

Over decades of research, time-frequency methods have emerged as the preferred approach, as time-domain-based methods are easily influenced by noise and pure frequency methods are not suitable for time-varying transients [76–78].

1.5. Wavelets for Fault Detection

Through extensive research, the wavelet transform is a very strong signal processing method for fault detection in HVDC systems, being well-suited to detect abrupt local changes in a signal [79]. Wavelet transforms can be grouped into two main categories: continuous wavelet transform (CWT) and discrete wavelet transform (DWT). CWT is used to measure how close the analysed signal is to the mother wavelet by using scaled and translated versions of the mother wavelet; this can be expressed by the following equation [80]:

$$CWT_{(a,b)} = \frac{1}{|a|^{\frac{1}{2}}} \int_{-\infty}^{\infty} x(n)\varphi\left(\frac{n-b}{a}\right)dn \quad (1)$$

where φ is a shifted and scaled version of the mother wavelet, a and b are the scale and time shift indices, respectively.

DWT uses features from both the time and frequency domains using multi-resolution analysis [81]. Signals are decomposed into approximated wavelet coefficients. C_{aj}, for low frequencies, and C_{dj}, for high frequency. This can be mathematically represented as shown below:

$$C_{aj}(e) = \sum fl_0(l_e - 2e)C_{aj-1}(l_e)$$

$$C_{dj}(e) = \sum fl_1(l_e - 2e)C_{aj-1}(l_e)$$

where fl_0 is the low-pass filter and fl_1 is the high-pass filter [82]. The mother wavelets used in DWT can be Daubechies (db), symlets (sym), and coiflets (coif) [82,83]. The wavelet coefficient is the cross-correlation of the signal and the mother wavelet, such that the higher the coefficient, the closer it matches the mother wavelet. Therefore, it is imperative that a suitable mother wavelet is chosen to match the pattern of the fault. Orthogonality, symmetry, vanishing moments, and support width can be used initially to check whether a mother wavelet is suitable. Orthogonality avoids decomposition redundancy and ensures unique reconstruction for energy finite signals. The symmetry property can avoid distortion in the decomposition of DWT. Vanishing moments are the most important property, as they show the decay rate of the wavelet. Support width is closely related to vanishing moments; the wider the support, the more information is getting into the decomposition part on a particular scale.

A small table comparing these properties is shown in Table 2 below [84–86].

Table 2. Comparison of wavelet properties.

Wavelets	Daubechies	Symlets
Orthogonal	Yes	Yes
Symmetry	Far from	Near from
Vanishing moments	N	N
Support width	2 N	2 N

2. Results Analysis

This paper aims to analyse the performance of various discrete wavelets for fault detection in HVDC systems to find the most suitable wavelets for the proposed application. For this purpose, a four-terminal VSC grid shown in Figure 4 is used for testing. This model was chosen as it is consistent with previous studies on this subject [68]. It is a VSC-based multi-terminal grid with two rectifiers and two inverters, where each rectifier is connected to the corresponding inverter by a 200 km cable. Furthermore, the two are interconnected with each other by 200 km cables. Finally, a load of 100 KΩ is added at the end to simulate external faults. The proposed study considers only DC faults in the transmission line. DC faults in such a system have been previously classified as follows [61]:

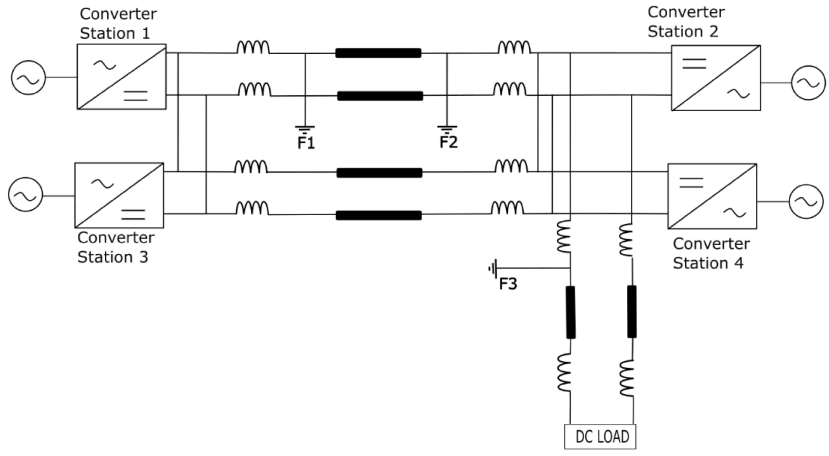

Figure 4. Four-terminal grid.

F1: Forward internal (Close-up) is positioned before the transmission line next to Rectifier 1.

F2: Forward internal (Remote), where the fault is positioned at the end of the transmission line.

F3: forward external fault, modelled on the load.

A protection algorithm proposed for such an application should be able to differentiate between internal and external faults so that a decision can be given to the relay whether to trip or not. To do so, a 5-level discrete wavelet transform is carried out on the current data from which the detail coefficient can then be extracted. The initial decision if a fault has or has not occurred is carried out by calculating the entropy of the current signal. The final decision of the algorithm to distinguish between an internal and an external fault is carried out using the threshold of the highest external fault coefficients.

Previous studies have shown wavelets as a suitable signal processing protection algorithm, and this study aims to investigate three mother wavelets, symlets, daubechies, and coiflets, to find the most fitting wavelet for each possible scenario. To do this, each wavelet is simulated under various noise conditions and cable lengths to determine the detection delay, the accuracy, and the processing time. The performance metrics can be defined as:

Detection delay—the delay between the time at the inception of the fault (at 0.3 s in this study) and the fault being detected.

Accuracy—the ratio between the number of correct detections against the number of correct and false detections.

Wavelet processing time—time taken to execute the algorithm script.

Figure 4 shows the four terminal grid used for the simulation study.

The study is presented in the following manner:

Firstly, the wavelets are simulated on the four-terminal grid shown above for no noise with cable lengths of 200 km, and the performance metrics defined before are found.

Power system environments generally present significant EMI and measurement noise. This can affect and compromise the accuracy of fault detection. Hence, the system shown in Figure 4 is also tested under various noise levels: 30 dB, 20 dB, and 10 dB for both F1 and F2 faults.

Additionally, further tests are carried for cable lengths of 50 km and 400 km under no noise to determine the effect of line distance on the protection algorithm.

Furthermore, modern power systems exhibit increasing complexity and heterogeneity with the integration of renewable energy sources, HVDC transmission and distributed generation. Key challenges include system complexities, variable operating conditions, and multi-terminal configurations. Fault detection techniques should therefore be adaptable to different systems. Consequently, the same tests carried out for the four-terminal grid are also carried out on a three-terminal grid to determine the adaptability of each wavelet. Finally, real-time solutions are provided to verify the four-node and three-node systems.

2.1. Four-Terminal Grid Experiencing No Noise

Figure 5 above shows the current rise for the internal close-up fault. A drastic current rise is observed at the inception of the fault.

Figure 6 above shows the current rise for the internal remote fault, and Figure 7 shows the effect of an external fault on the system. Similarly, the fault rises at the fault inception time, but the amplitude of the current is lower due to the distance between the location of the fault and the relay. Table 3 below shows a comparison between the wavelets, and it depicts the results for the four-terminal grid with cable lengths of 200 km with no noise.

Figure 8 shows the radar charts for F1 and F2, respectively, for the four-terminal system with cable lengths of 200 km under no noise. These radar charts are normalised so

that all the performance metrics can be shown together to better grasp which wavelet is more suitable for each scenario.

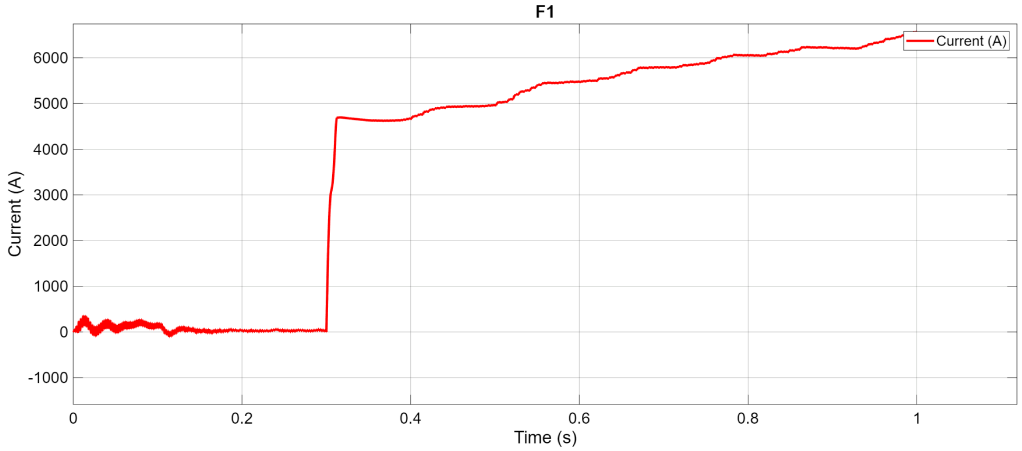

Figure 5. Internal close−up fault (F1).

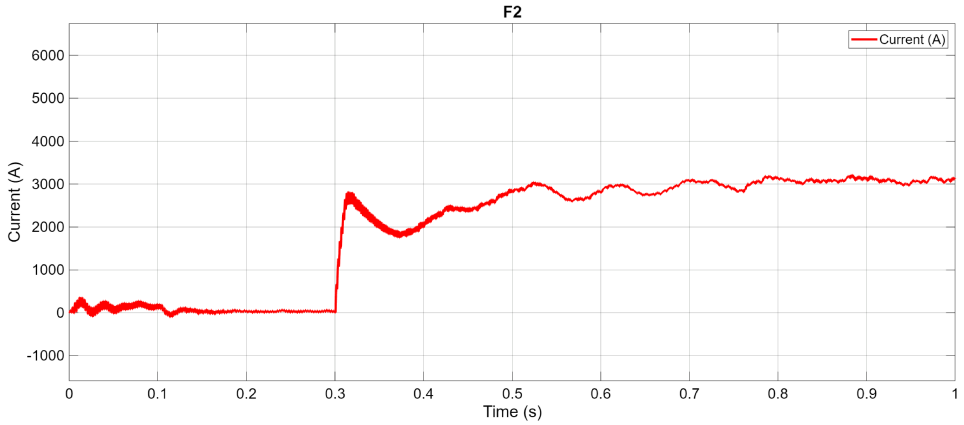

Figure 6. Internal remote fault (F2).

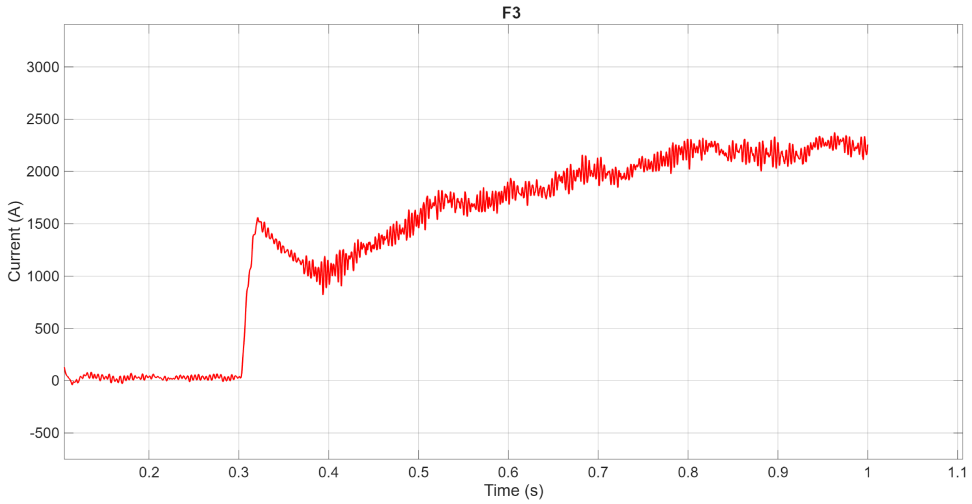

Figure 7. External fault (F3).

For this system, when an F1 fault occurs on the system, it is found that db4 provides the best outcome with the least detection delay and highest accuracy. However, when a remote internal fault is modelled, it is found that the wavelet's detection delay is increased and is no longer the clear choice. From Table 2, a general trend can be observed where the accuracy is greatly reduced for an F2, and the detection delay is increased. For such a

system, the choice of wavelet lies between sym3 and db4. Additionally, the computational burden and entropy value are found to be almost the same for every wavelet.

Table 3. Performance under no noise.

F1	Wavelet	Detection Delay ms	Accuracy %	F2	Wavelet	Detection Delay ms	Accuracy %
	sym3	2.07	85		sym3	2.07	68
	db4	1.11	87		db4	2.69	72
	coif3	2.65	86		coif3	2.65	68
	coif5	6.28	85		coif5	4.75	66
	db8	3.6	85		db8	5.2	67
	sym5	1.74	84		sym5	3.32	67

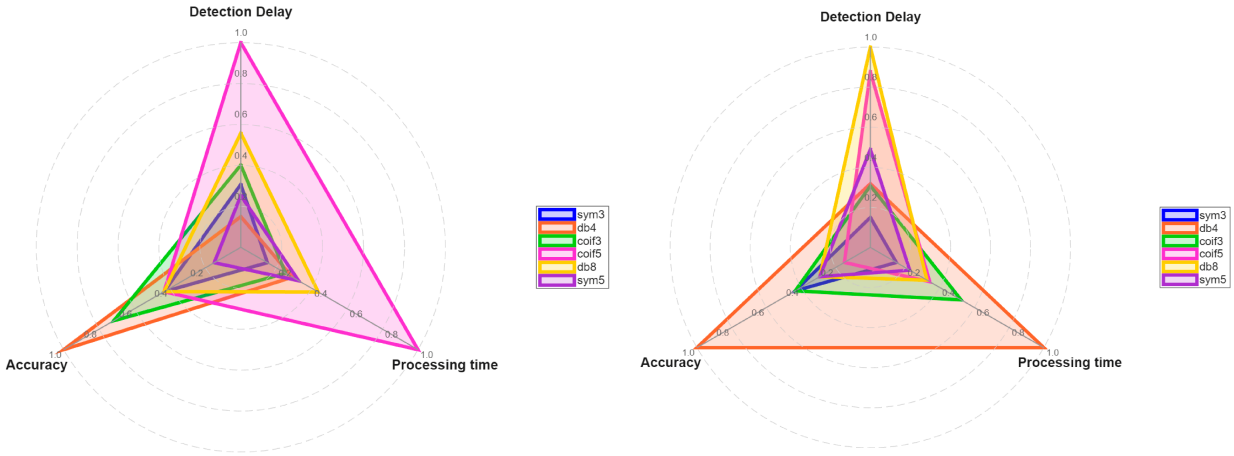

(**a**) (**b**)

Figure 8. Radar chart of a four-terminal grid under no noise for (**a**) F1 and (**b**) F2.

To assess each wavelet's susceptibility to noise, white Gaussian noise with a signal-to-noise ratio (SNR) of 30 dB, 20 dB, and 10 dB is introduced to the input signal. SNR values of 30 dB and 20 dB are found to be the widely used values to measure noise in a transmission line [87–90], where a lower SNR value signifies a higher noise environment. Therefore, a system under an SNR of 10 dB is also modelled to analyse the behaviour of the wavelets under extreme noise conditions.

2.2. Four-Terminal Grid Experiencing 30 dB Noise

Figure 9 above shows the behaviour of the F1 current rise when a 30 dB noise is experienced, and Figure 10 below shows the radar charts for F1 and F2 under 30 dB noise. When considering a system under noise, the threshold for distinguishing between external and internal faults can vary, as the noise is never the same. This causes irregular data values, sometimes causing misclassifications or pre-transient detections. From Figure 8, it could be deduced that sym3 is the best wavelet for fault detection under these noise conditions, but this is an anomaly caused by the noise. For such a condition, the choice is between coif3, db8, and sym5. Coif3 offers the least delay with the highest accuracy for F1, which can be compared to the performance of some wavelets under no noise.

However, this is not the case when considering an F2 fault, where, although the accuracy is still competitive, the delay is much higher, rendering it unusable for such cases. Unlike coif3, db8 is consistent in delay for both F1 and F2 but has a lower accuracy than coif3. Finally, sym5 has a lower delay than db8 when considering an F1 fault, but a higher delay when an F2 is modelled for the same accuracy. Under these conditions, the most suitable wavelet would be db8.

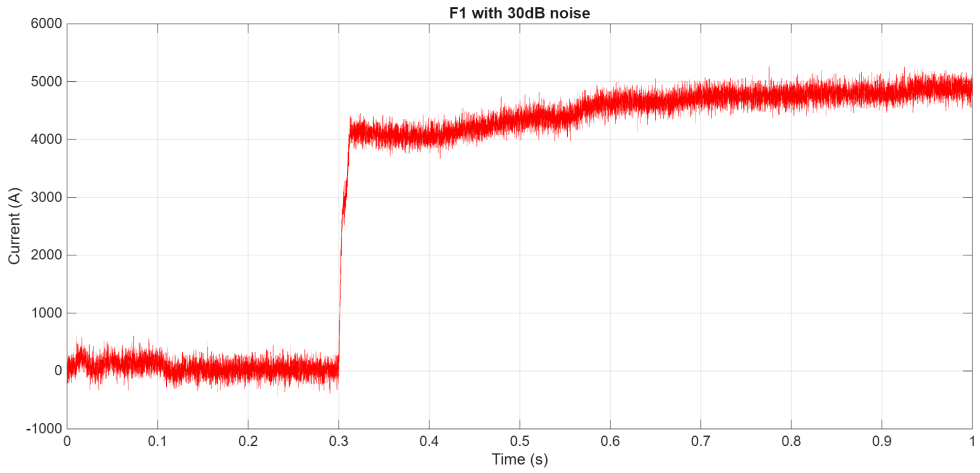

Figure 9. F1 with 30 dB noise.

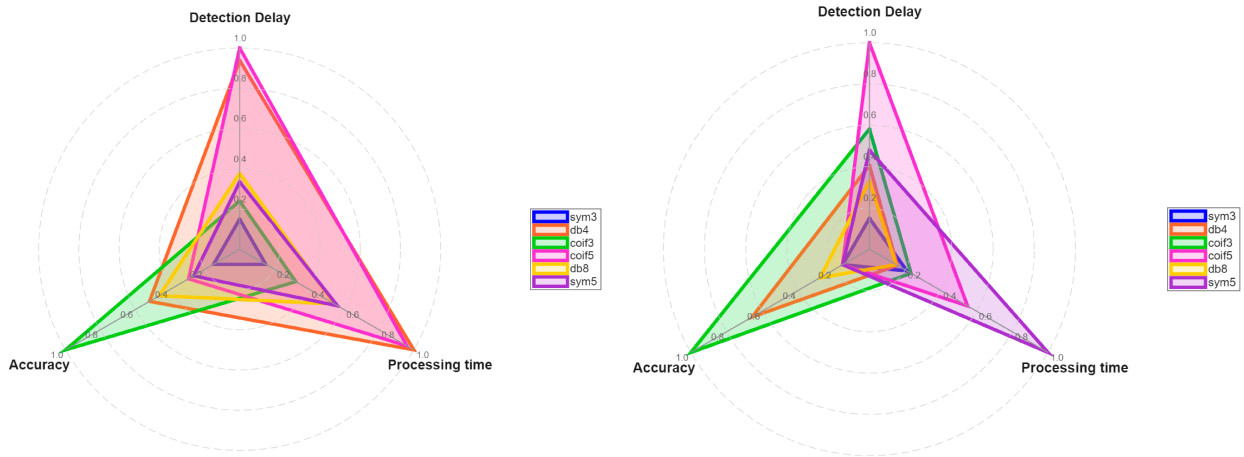

(**a**) (**b**)

Figure 10. Radar chart of a four-terminal grid under 30 dB for (**a**) F1 and (**b**) F2.

2.3. Four-Terminal Grid Experiencing 20 dB Noise

Now, considering the same four-terminal grid under 20 dB, the plots shown in Figure 11 below were obtained. From the obtained plots above, it can be seen that db8 is the least suitable wavelet under the 20 dB noise conditions, having high detection delays. However, coif5 can be said to be worse, even though the plot shows good performance. This is due to pre-transient detection, making this wavelet susceptible to noise under the considered 20 dB conditions. For these, sym5, db4, and coif3 can be recommended, as coif3 shows the least delay under an F2 fault, but when considering an F1 fault, the delay is increased. Whereas sym5 has unchanged delay for both F1 and F2, for only a slight increase in the delay, with a slightly better accuracy. Similarly, db4 also has consistent delay over both F1 and F2; however, this time the detection delay is much higher than coif3, but db4 offers noticeably higher accuracy. Therefore, the recommended wavelet for 20 dB noise of a four-terminal grid is between sym5, db4, and coif3.

2.4. Four-Terminal Grid Experiencing 10 dB Noise

Finally, considering the same system under 10 dB noise, the comparison plots are shown below in Figure 12. As expected, a high drop in accuracy was recorded during the simulations, with the accuracy of db4 and coif5 going down to 35% and 38%. For Fault 2, two wavelets, coif3 and db8, recorded a very unexpectedly high accuracy. However, it was found that these two wavelets often misclassify between internal and external faults,

which compels that these high accuracies are anomalies. Although the accuracy of the two wavelets mentioned above (db4, coif5) are very low, they exhibited the least detection delay. Therefore, these two are the best wavelets for such conditions, as the others either exhibit pre-transient errors or misclassify the fault.

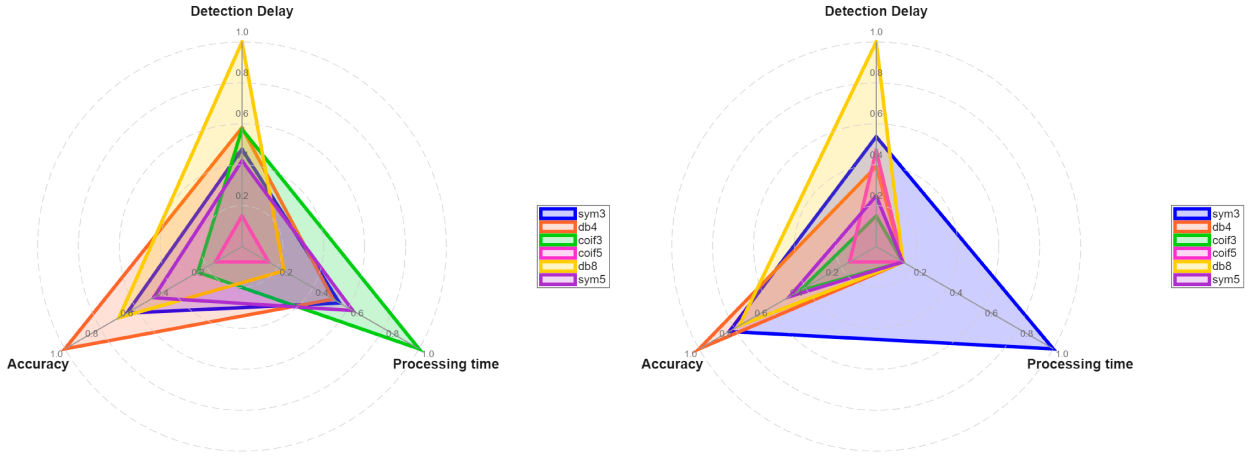

Figure 11. Radar chart of a four-terminal grid under 20 dB for (**a**) F1 and (**b**) F2.

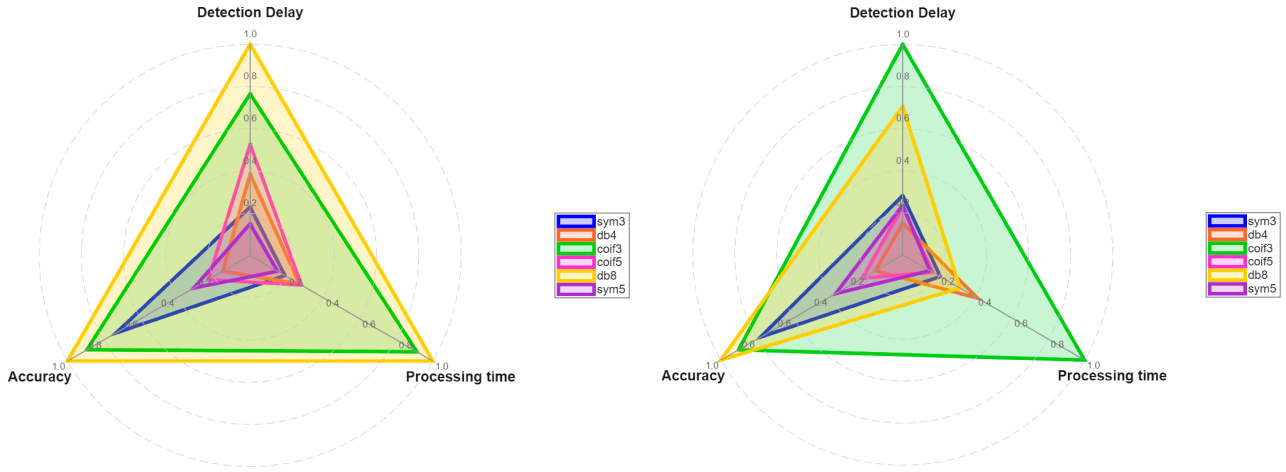

Figure 12. Radar chart of a four-terminal grid under 10 dB for (**a**) F1 and (**b**) F2.

Overall, considering a four-terminal grid under a noisy environment, the following conclusions can be made for each wavelet. The least susceptible to noise is db4, maintaining a consistent detection delay throughout, with accuracies not too far behind other wavelets. The most susceptible to noise under these conditions is sym3, which constantly reported pre-transient errors due to noise. Coif5, db8, and coif3 are also not recommended, even though they have exhibited consistent behaviour; the detection delays are too high to be considered in real-life situations, with some wavelets such as db8 even misclassifying between internal and external fault, triggering the circuit breaker.

Another wavelet that can be recommended is sym5, which showed good performance overall with low detection delays and high accuracy in comparison to the other wavelets. To evaluate the adaptability of the wavelets, tests were conducted for different cable lengths of 50 km and 400 km.

2.5. Four-Terminal Grid with Cable Length of 50 km

Below in Figure 13 are the radar charts for F1 and F2 for the same four-terminal grid shown in Figure 4, but now with a cable length of 50 km under no noise. From these plots, the two recommended wavelets are db4 and sym3, with db4 having the least delay over both F1 and F2, but with lower accuracy than sym3, as sym3, although having a higher detection delay, also has a higher accuracy in both the faults. Sym5 is the least suitable for a 50 km cable length scenario as it experiences pre-transient detections, which can be destructive in real-life scenarios.

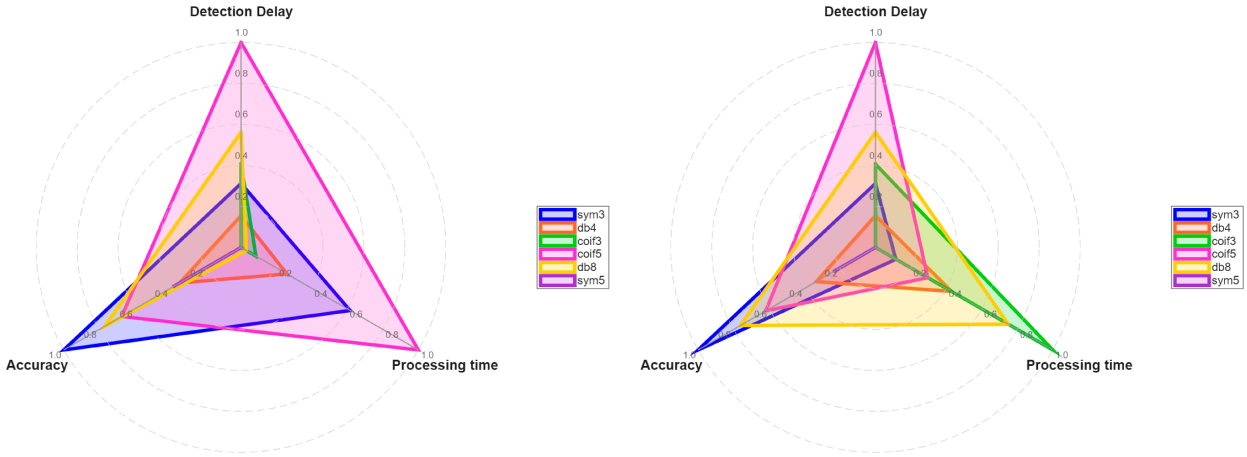

Figure 13. Four-terminal grid with cable lengths of 50 km.

2.6. Four-Terminal Grid with Cable Length of 400 km

Finally, the cable lengths are changed to 400 km, where the wavelets experience irregular results. The results are shown in Figure 14. Due to the long distance when a remote fault is experienced, the accuracy is much lower than the accuracy of a close-up fault, dropping nearly 60%. Throughout the test for the 400 km scenario, sym3 is the best, as it displays consistent detection delay through both F1 and F2, having the highest accuracy relative to other wavelets. Another recommended wavelet for the 400 km scenario is sym5, which, although it has a slightly lower accuracy throughout both faults, also experiences the least detection delay. Therefore, the symlet mother wavelet is the best when considering such long distances, as they have the best and most consistent results throughout the test, whereas the other wavelets experience a drastic increase in detection delay and decrease in accuracy.

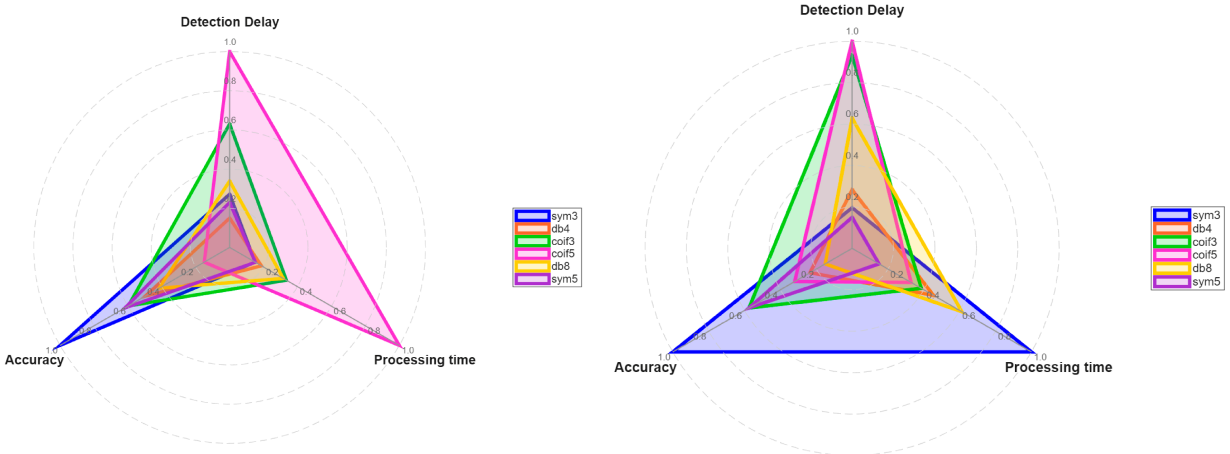

Figure 14. Four-terminal grids with cable lengths of 400 km.

2.7. Three-Terminal Grid Experiencing No Noise

To further test the adaptability, the same tests carried out for the four terminals are applied on a three-terminal grid, as shown in Figure 15.

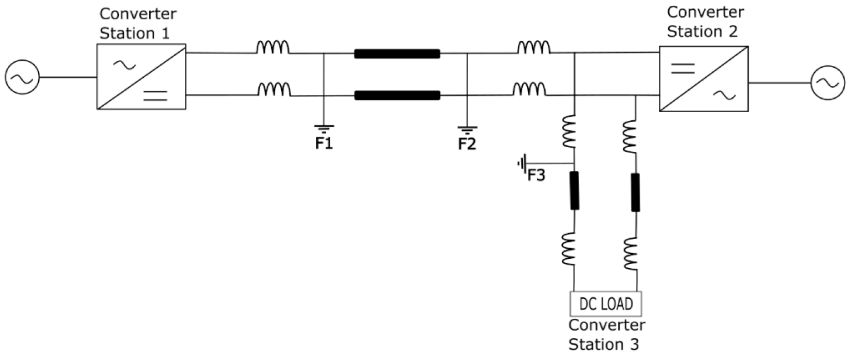

Figure 15. Three-terminal grids.

Figure 16a,b below shows the noise-free graphs for F1 and F2 faults for the three-terminal grid, and the radar chart with the same noise conditions for a four-terminal grid is shown in Figure 8a,b. Comparing the two, sym3 wavelet is the most adaptable for the depicted conditions, with a consistent delay over both the three-terminal and four-terminal grids, with competing accuracy in the four-terminal grid and the highest accuracy in the three-terminal grid. Additionally, coif5 is the worst considering no noise conditions in the three-terminal grid, where the detection delay is already high, and it further increases.

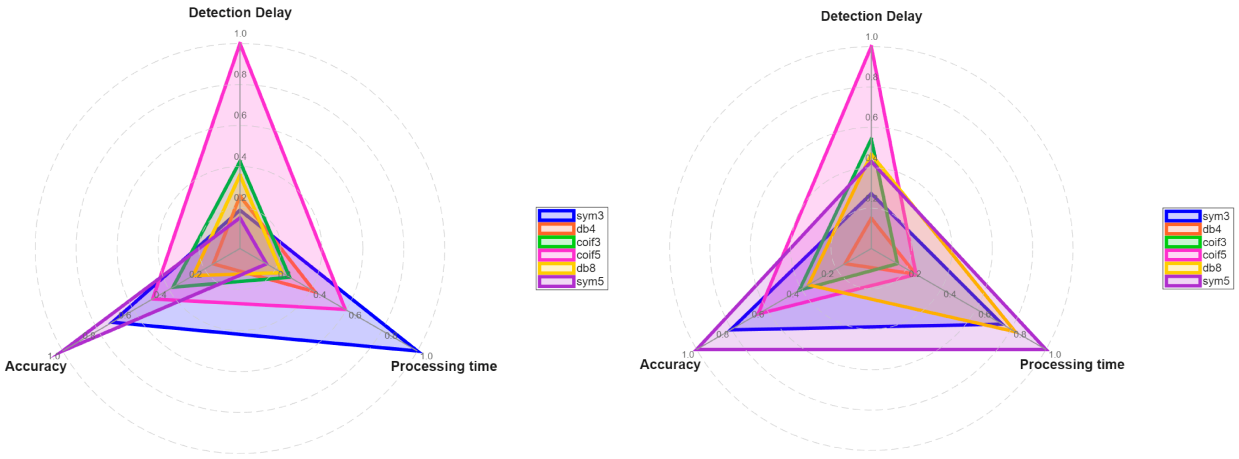

(**a**) (**b**)

Figure 16. Radar chart of a three-terminal grid under no noise for (**a**) F1 and (**b**) F2.

2.8. Three-Terminal Grid Experiencing 30 dB Noise

For a three-terminal grid under 30 dB noise, sym3 retains its detection delay when noise is added, with a consistent detection delay of 2.07 ms for both F1 and F2 with high accuracy. This can also be seen below in Figure 17, where sym3 has the least detection delay for both the F1 and F2 faults.

2.9. Three-Terminal Grid Experiencing 20 dB Noise

Sym3 continues to be the best choice even when testing for a higher noise environment (under 20 dB). From Figure 18a below, we can see that db8 seems to be the best choice. The reason db8 shows the least delay is due to pre-transient detection; this can also be seen from the poor accuracy shown by db8. From Figure 18b, db4 could be said to be the best choice, as it has the least detection delay; however, when looking at the performance of

db4 on the F1 fault, it has the highest detection delay with the least accuracy, making it non-viable for fault detection under these conditions.

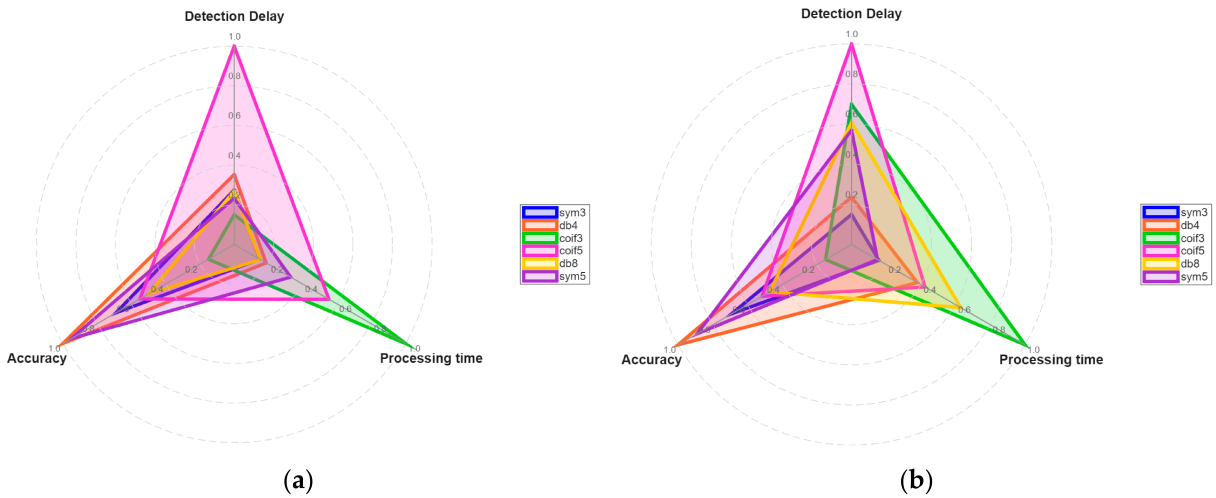

Figure 17. Radar chart of a three-terminal grid under 30 dB for (**a**) F1 and (**b**) F2.

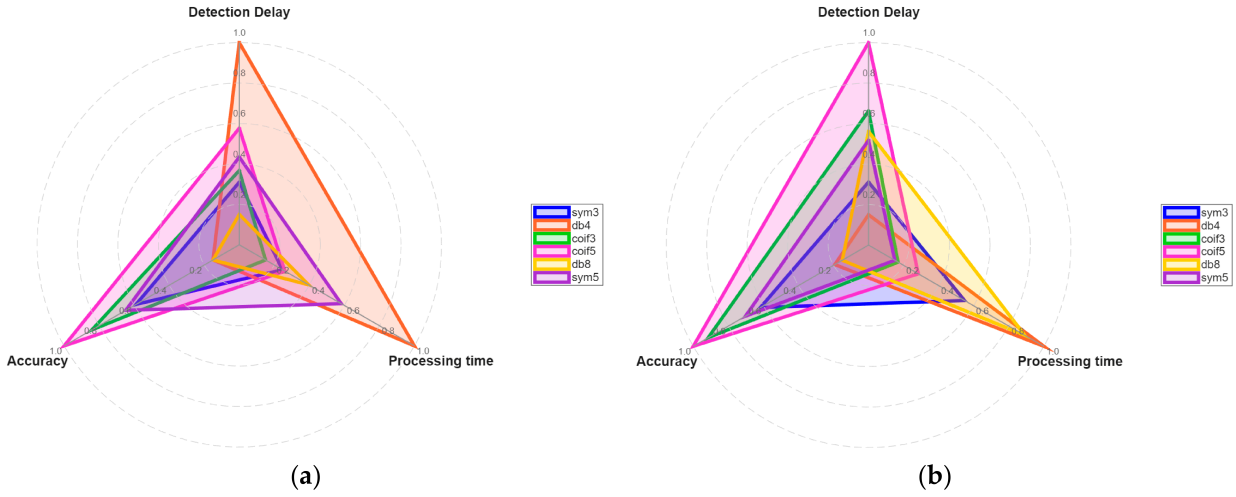

Figure 18. Radar chart of a three-terminal grid under 20 dB for (**a**) F1 and (**b**) F2.

2.10. Three-Terminal Grid Experiencing 10 dB Noise

When considering the system under 10 dB noise, many problems arise. The results are shown in Figure 19. Where coif5 misclassifies faults due to the extreme noise, db4 has pre-transient detection errors, and sym5, db8, and coif3 show anomalies in the detection accuracies. Considering these facts, only sym3 can be considered for fault detection in such conditions, even though detection delay can go as high as 9 ms and accuracy as low as 44%.

Finally, considering a three-terminal system, sym3 is the recommended wavelet, as it has the least detection delay, is the least susceptible to noise, and has acceptable accuracies throughout the tests.

Overall, when considering a multi-terminal grid and a noisy environment, the only recommendable wavelets for fault detection are db4 and sym3, as sym3 has proven to be the most adaptable of the wavelets and db4 has shown the least detection delay. Furthermore, the tests have proven that db4 is the best if considering a four-terminal grid under any kind of noise, whereas sym3 proved to be the choice for any noise scenario in a three-terminal grid. A summary of the work is presented in Table 4 below.

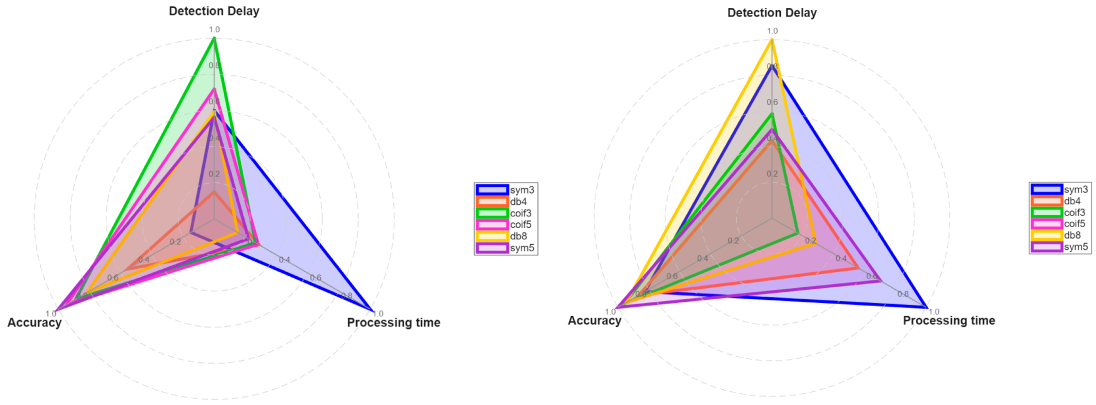

(**a**) (**b**)

Figure 19. Radar chart of a three-terminal grid under 10 dB for (**a**) F1 and (**b**) F2.

Table 4. Recommended wavelet based on each scenario.

System Scenario	Recommended Wavelet
Four-terminal no noise	Sym3, db4
Four-terminal 30 dB noise	Db8
Four-terminal 20 dB noise	Sym5, db4, coif3
Four-terminal 10 dB noise	Db4, coif5
Four-terminal 50 km	Db4, sym3
Four terminal 400 km	Sym3, sym5
Three-terminal no noise	Sym3
Three-terminal 30 dB noise	Sym3
Three-terminal 20 dB noise	Sym3
Three-terminal 10 dB noise	Sym3

2.11. Statistical Analysis

In this section, statistical analysis is performed to provide quantitative features of the experiment carried out. Table 5 shows the 3 factor ANOVA test carried out for detection delay. Furthermore, a 95% confidence interval is performed to enhance the objectivity of the experiment for detection delay, as shown in Table 6.

Table 5. Three-factor ANOVA for the time taken to detect the fault.

Source	Sum Sq.	Mean Sq.	F	*p*-Value
Fault Type	8.619	8.6	2.79	0.1
Noise	4.96	1.65	0.53	0.6642
Wavelet	43.456	8.71	2.79	0.0303

Table 6. Ninety-five percent confidence intervals for the time taken to detect the fault.

Source	Mean	CI Lower	CI Upper
F1	2.46	1.73	3.19
F2	3.31	2.52	4.09
No Noise	3.18	2.31	4.05
30 dB Noise	3.17	1.81	4.52
20 dB Noise	2.80	1.79	3.80
10 dB Noise	2.40	1.23	3.56
Sym3	1.67	0.89	2.45
Db4	2.49	1.41	3.58
Coif3	3.04	1.66	4.42
Coif5	3.98	2.10	5.86
Db8	4.19	3.06	5.34
Sym5	1.94	1.24	2.64

Finally, Tables 7 and 8 show the 3 factor ANOVA test for the accuracy and the 95% confidence interval respectively.

Table 7. ANOVA test for accuracy.

Source	Sum Sq.	Mean Sq.	F	*p*-Value
Fault Type	1021	1021	6.54	0.0146
Noise	1087	362	2.32	0.0907
Wavelet	868.85	174	1.11	0.3699

Table 8. Ninety-five percent confidence interval for accuracy.

Source	Mean	CI Lower	CI Upper
F1	64	57.83	71
F2	73	70	77
No Noise	77	71	82
30 dB Noise	68	64	71
20 dB Noise	67	59	75
10 dB Noise	64	53	75
Sym3	70	61	79
Db4	68	57	80
Coif3	74	65	83
Coif5	62	52	72
Db8	73	65	82
Sym5	65	56	74

Below in Table 5, the ANOVA test results for detection are shown. It can be seen that the type of wavelet has a significant effect on the detection delay, whereas the noise and fault type do not.

Table 6 below shows a 95% confidence interval test for the detection delay. The effect of each individual source on the detection delay is measured. Additionally, the mean detection delay is shown with the lower bound confidence interval and the upper bound confidence interval. From Table 6, it is possible to see that when using sym3, the detection delay is the lowest overall when considering any type of noise with any type of fault.

Table 7 below shows the ANOVA test results for the accuracy of the experiment. As seen below, the fault type has a significant effect on the accuracy, whereas the noise does not have a significant effect and the type of wavelet has a very low effect on the accuracy.

Table 8 below shows the 95% confidence interval carried out for the accuracy of the experiment. As seen below, the accuracy is the highest when considering a no noise environment and the lowest when considering the 10 dB noise. Coif5 provides the least accuracy over all types of faults and all types of noise, and coif3 provides the highest overall accuracy.

3. Real-Time Hardware in the Loop Verification

To provide a real-time verification of the test, the same model used in SIMULINK was tested on the OPAL-RT, an FPGA hardware in the loop (HIL) used to test models in real time. A block diagram of the setup is shown below in Figure 20.

Below in Figure 21, the current graph for a close-up internal fault is shown; it can be seen that, similar to the offline situation, the current graph spikes at a fault inception time of 0.3 s. Furthermore, it can be seen that the OPAL-RT models the noisy environment, further emphasising the need to test the behaviour of the wavelets under different noise conditions.

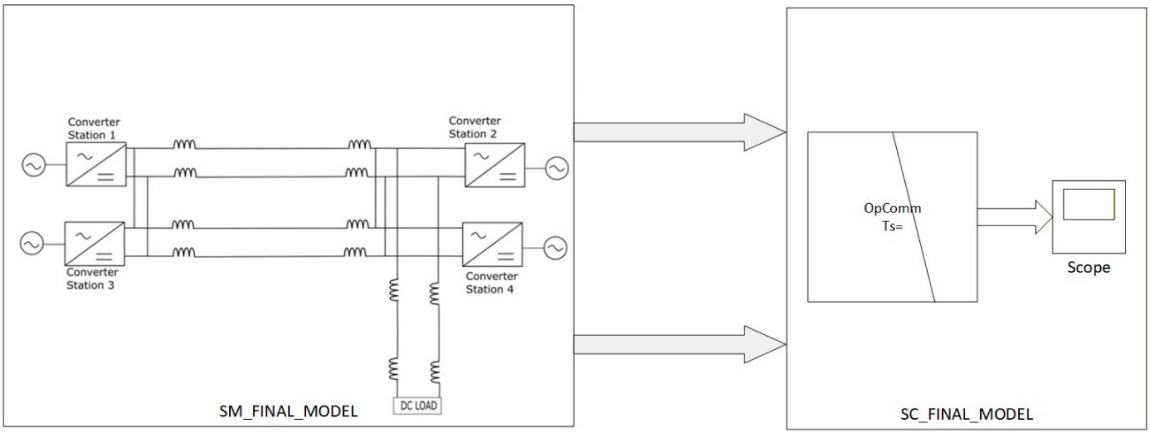

Figure 20. Real-time set up on OPAL-RT.

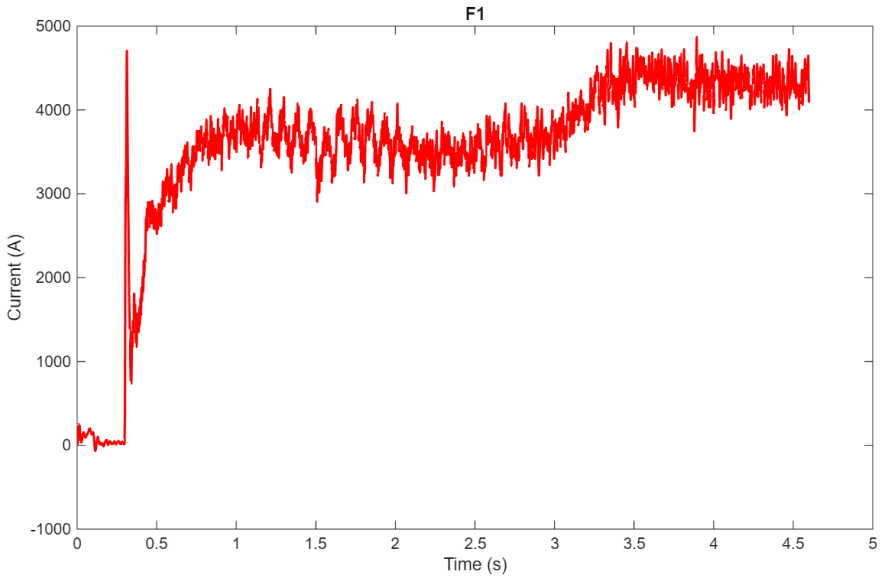

Figure 21. Real-time verification of F1.

In Figure 22, the current graph for a remote internal fault is shown.

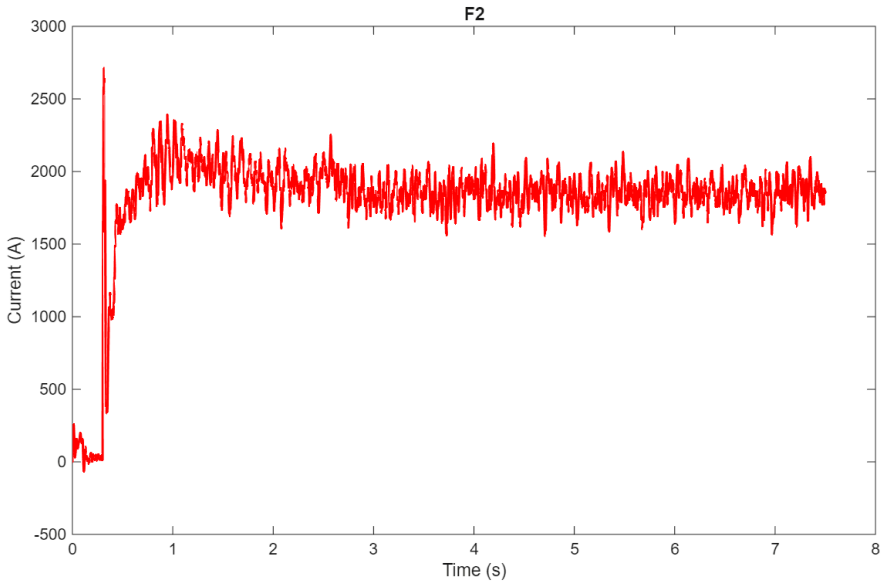

Figure 22. Real-time verification of F2.

In Figure 23 below, the real-time verification of an external fault carried out on OPAL-RT is shown.

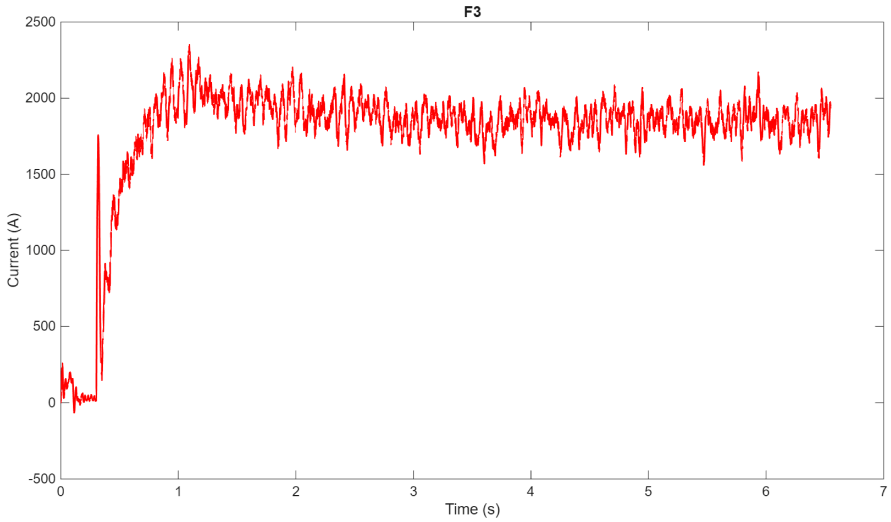

Figure 23. Real-time verification of F3.

4. Conclusions

This paper presents a systematic performance comparison of six discrete wavelet mother wavelets, namely db4, db8, sym3, sym5, coif3, and coif5, for DC fault detection in multi-terminal VSC-HVDC grids, evaluated across both four-terminal and three-terminal configurations under varying noise conditions and cable lengths. The study assessed each wavelet against four key performance metrics, detection delay, classification accuracy, noise tolerance, and computational efficiency, with real-time validation performed on an OPAL-RT hardware-in-the-loop platform.

The results demonstrate that no single wavelet universally outperforms across all operating conditions; rather, the optimal selection is governed by the specific grid topology, noise environment, and cable length.

For four-terminal VSC-HVDC grids operating under low-noise or noise-free conditions, db4 is the recommended wavelet, offering the lowest detection delay and consistently high classification accuracy for both close-up internal (F1) and remote internal (F2) faults. As the noise severity increases, sym5 and coif3 present viable alternatives at moderate noise levels (20 dB SNR), while db4 retains its suitability even under high-noise conditions (10 dB SNR) alongside coif5. Conversely, sym3 exhibited the highest susceptibility to noise in four-terminal configurations, frequently producing pre-transient detection errors under noisy conditions.

For three-terminal VSC-HVDC grids, sym3 emerged as the consistently recommended wavelet across all tested noise levels and fault types. Despite exhibiting a marginally higher detection delay compared to db4 under no-noise conditions, sym3 demonstrated superior robustness to noise and maintained acceptable accuracy throughout, making it the most adaptable and reliable choice for three-terminal deployment. This distinction underscores the importance of topology-aware wavelet selection in the design of DWT-based protection schemes.

The cable length was further shown to be a significant determinant of wavelet performance. At shorter cable lengths (50 km), db4 and sym3 were found to be the most effective, whereas at extended distances (400 km), symlet wavelets, particularly sym3 and sym5, demonstrated the most consistent performance, maintaining the detection delay and accuracy where other wavelet families exhibited marked degradation. These findings highlight

the critical sensitivity of wavelet-based protection algorithms to transmission line parameters and reinforce the necessity of site-specific optimisation in practical deployments.

The real-time verification conducted on the OPAL-RT HIL platform validated the offline simulation results, confirming that the current signatures and detection behaviours observed in MATLAB/Simulink are reproducible under real-time conditions. Importantly, the real-time environment further demonstrated the inherent noise present in physical power systems, lending additional weight to the study's emphasis on noise tolerance as a primary selection criterion.

The findings of this study provide clear, evidence-based guidelines for the nuanced selection of discrete wavelet mother wavelets in DWT-based protection algorithms for multi-terminal VSC-HVDC systems. The overall recommendation is that db4 be adopted for four-terminal grid applications where detection speed is the primary concern, while sym3 is best suited to three-terminal configurations and long-distance transmission scenarios requiring robustness under adverse noise conditions. Future work should extend this comparative framework to larger meshed HVDC networks, incorporate additional fault resistance levels and fault types, and look into hybrid signal processing approaches that combine the complementary strengths of multiple wavelet families to further enhance protection performance.

Author Contributions: Conceptualisation, Methodology, Software, Validation, Writing—original draft, Formal analysis, Resources, A.S.; Conceptualisation, Methodology, Software, Validation, Formal analysis, Writing—original draft, Data curation, Supervisor, M.J.; Conceptualisation, Investigation, Methodology, Software, Validation, Formal analysis, Writing—original draft, M.N.I.; Investigation, Resources, Data curation, Writing—review & editing, Formal analysis, Visualisation, K.D.; Investigation, Visualisation, Resources, Data curation, Validation, Writing—review & editing, H.A.R.; Writing—review & editing, Visualisation, Investigation, Resources, Software, Formal analysis, R.A.Q.; Writing—review & editing, Supervision, Data curation, Project administration, Funding acquisition, Resources, Visualisation, N.S. All authors have read and agreed to the published version of the manuscript.

Funding: This research received no external funding.

Data Availability Statement: The data are available on request.

Conflicts of Interest: The authors declare no conflicts of interest.

References

1. Wired for Climate Neutrality—A Paris Agreement Compatible (PAC) Roadmap for Power Grids. Available online: https://eeb.org/library/wired-for-climate-neutrality-a-paris-agreement-compatible-pac-roadmap-for-power-grids/ (accessed on 13 November 2025).
2. Alassi, A.; Bañales, S.; Ellabban, O.; Adam, G.; MacIver, C. HVDC Transmission: Technology Review, Market Trends and Future Outlook. *Renew. Sustain. Energy Rev.* **2019**, *112*, 530–554. [CrossRef]
3. Ahmed, N.; Ram, N.; Memon, A.P.; Ahmed, S. Comparative Analysis of Fault Detection for HVDC Transmission System Using Wavelet Transform Based on Standard Deviation. In Proceedings of the 2020 3rd International Conference on Computing, Mathematics and Engineering Technologies: Idea to Innovation for Building the Knowledge Economy, iCoMET 2020, Sukkur, Pakistan, 29–30 January 2020. [CrossRef]
4. Long, W.; Nilsson, S. HVDC Transmission: Yesterday and Today. *IEEE Power Energy Mag.* **2007**, *5*, 22–31. [CrossRef]
5. Woodford, D. *HVDC Transmission*; Wydawnictwo Uniwersytetu Morskiego Gdyni: Gdynia, Poland, 1998.
6. Watson, N.R.; Watson, J.D. An Overview of HVDC Technology. *Energies* **2020**, *13*, 4342. [CrossRef]
7. Lips, H.P. Technology Trends for HVDC Thyristor Valves. In Proceedings of the POWERCON 1998—1998 International Conference on Power System Technology, Proceedings, Beijing, China, 18–21 August 1998; Volume 1, pp. 451–455. [CrossRef]
8. Pierri, E.; Binder, O.; Hemdan, N.G.A.; Kurrat, M. Challenges and Opportunities for a European HVDC Grid. *Renew. Sustain. Energy Rev.* **2017**, *70*, 427–456. [CrossRef]

9. Rodrigues, E.; Pontes, R.S.T.; Bandeira, J.; Aguiar, V.P.B. Analysis of the Incidence of Direct Lightning over a HVDC Transmission Line through EFD Model. *Energies* **2019**, *12*, 555. [CrossRef]
10. Qin, X.; Zeng, P.; Zhou, Q.; Dai, Q.; Chen, J. Study on the Development and Reliability of HVDC Transmission Systems in China. In Proceedings of the 2016 IEEE International Conference on Power System Technology, POWERCON 2016, Wollongong, Australia, 24 November 2016. [CrossRef]
11. Ikhide, M.A. DC Line Protection for Multi-Terminal High Voltage DC (HVDC) Transmission Systems. Ph.D. Thesis, Staffordshire University, Stoke-on-Trent, UK, 2017.
12. Meah, K.; Ula, S. Comparative Evaluation of HVDC and HVAC Transmission Systems. In Proceedings of the 2007 IEEE Power Engineering Society General Meeting, PES, Tampa, FL, USA, 24–28 June 2007. [CrossRef]
13. Hussein, I.I.; Essallah, S.; Khedher, A. Comparative Study of HVDC and HVAC Systems in Presence of Large Scale Renewable Energy Sources. In Proceedings of the STA 2020: 2020 20th International Conference on Sciences and Techniques of Automatic Control and Computer Engineering, Monastir, Tunisia, 20–22 December 2020; pp. 225–230. [CrossRef]
14. Johannesson, K.; Gustafsson, A.; Karlstrand, J.; Jeroense, M. *HVDC Light Cables for Long Distance Grid Connection*; ASEA Brown Boveri: Stockholm, Sweden, 2009.
15. Kalair, A.; Abas, N.; Khan, N. Comparative Study of HVAC and HVDC Transmission Systems. *Renew. Sustain. Energy Rev.* **2016**, *59*, 1653–1675. [CrossRef]
16. Lundkvist, J.; Gutman, I.; Weimers, L. Feasibility Study for Converting 380 KV AC Lines to Hybrid AC/DC Lines. In Proceedings of the EPRI's High-Voltage Direct Current & Flexible AC Transmission Systems Conference, Westminster, CO, USA, 15–17 September 2009.
17. Kim, C.K.; Sood, V.K.; Jang, G.S.; Lim, S.J.; Lee, S.J. *HVDC Transmission: Power Conversion Applications in Power Systems*; Wiley: Hoboken, NJ, USA, 2010. [CrossRef]
18. GE Vernova. DC Transmission Systems: Line Commutated Converters. Available online: https://library.grid.gevernova.com/hvdc/hdvc-lcc-reference-book (accessed on 13 November 2025).
19. Jovcic, D. *High Voltage Direct Current Transmission: Converters, Systems and DC Grids, Second Edition*; Wiley: Hoboken, NJ, USA, 2019; pp. 1–537. [CrossRef]
20. Rudervall, R.; Charpentier, J.; Sharma, R.Y. High Voltage Direct Current (HVDC) Transmission Systems Technology Review Paper. *Energy Week* **2000**, *2000*, 1–19.
21. Prof Barry Wayne Williams. *Principles and Elements of Power Electronics*; Springer: Berlin/Heidelberg, Germany, 2006.
22. Oni, O.E.; Mbangula, K.I.; Davidson, I.E. A Review of LCC-HVDC and VSC-HVDC Technologies and Applications. *Trans. Environ. Electr. Eng.* **2016**, *1*, 68. [CrossRef]
23. Hitachi Energy. *Longdong-Shandong UHVDC*; Hitachi Energy: Zurich, Switzerland, 2025.
24. Barsali, S.; Carlini, E.M.; Scirocco, T.B.; Pisaneschi, F.; Urbanelli, A.; Belmonte, L. Hybrid HVDC LCC-VSC System Integration and Technological Aspects in a Multi-Terminal DC Grid. In Proceedings of the 2022 AEIT International Annual Conference, AEIT 2022, Rome, Italy, 3–5 October 2022. [CrossRef]
25. Guo, C.; Liu, Y.; Zhao, C.; Wei, X.; Xu, W. Power Component Fault Detection Method and Improved Current Order Limiter Control for Commutation Failure Mitigation in HVDC. *IEEE Trans. Power Deliv.* **2015**, *30*, 1585–1593. [CrossRef]
26. Mirsaeidi, S.; Tzelepis, D.; He, J.; Dong, X.; Said, D.M.; Booth, C. A Controllable Thyristor-Based Commutation Failure Inhibitor for LCC-HVDC Transmission Systems. *IEEE Trans. Power Electron.* **2021**, *36*, 3781–3792. [CrossRef]
27. Jiang-Hafner, Y.; Duchen, H.; Karlsson, M.; Ronstrom, L.; Abrahamsson, B. HVDC with Voltage Source Converters—A Powerful Standby Black Start Facility. In Proceedings of the Transmission and Distribution Exposition Conference: 2008 IEEE PES Powering Toward the Future, PIMS 2008, Chicago, IL, USA, 21–24 April 2008. [CrossRef]
28. CIGRE Working Group B4.37. *VSC Transmission*; Electra No.219; CIGRE: Paris, France, 2005.
29. Arrillaga, J.; Liu, Y.H.; Watson, N.R. *Flexible Power Transmission: The HVDC Options*; Wiley: Hoboken, NJ, USA, 2007; pp. 1–362. [CrossRef]
30. Wang, M.; An, T.; Ergun, H.; Lan, Y.; Andersen, B.; Szechtman, M.; Leterme, W.; Beerten, J.; Van Hertem, D. Review and Outlook of HVDC Grids as Backbone of Transmission System. *CSEE J. Power Energy Syst.* **2021**, *7*, 797–810. [CrossRef]
31. Barnes, M.; Beddard, A. Voltage Source Converter HVDC Links—The State of the Art and Issues Going Forward. *Energy Procedia* **2012**, *24*, 108–122. [CrossRef]
32. Daniel, K.; Kütt, L.; Iqbal, M.N.; Shabbir, N.; Parker, M.; Jarkovoi, M. Waveform Variation Defined Model for Harmonic Current Emissions Including Cross-Order Supply Voltage Harmonics Influence. *IEEE Access* **2023**, *11*, 42276–42289. [CrossRef]
33. Li, X.; Xu, Y.; Zhang, H.; Gao, Z. Control and Protection System Design of Zhangbei VSC-HVDC Grid. In Proceedings of the 2021 6th Asia Conference on Power and Electrical Engineering, ACPEE 2021, Chongqing, China, 8–11 April 2021; pp. 119–123. [CrossRef]
34. ABB Group R&D and Technology. *60 Years of HVDC (Special Report)*; ABB Group R&D and Technology: Zurich, Switzerland, 2014.

35. Friedrich, K. Modern HVDC PLUS Application of VSC in Modular Multilevel Converter Topology. In Proceedings of the 2010 IEEE International Symposium on Industrial Electronics, Bari, Italy, 4–7 July 2010; pp. 3807–3810. [CrossRef]
36. Alyami, H.; Mohamed, Y. Review and Development of MMC Employed in VSC-HVDC Systems. In Proceedings of the Canadian Conference on Electrical and Computer Engineering, Windsor, ON, Canada, 30 April–3 May 2017. [CrossRef]
37. Allebrod, S.; Hamerski, R.; Marquardt, R. New Transformerless, Scalable Modular Multilevel Converters for HVDC-Transmission. In Proceedings of the PESC Record-IEEE Annual Power Electronics Specialists Conference, Rhodes, Greece, 15–19 June 2008; pp. 174–179. [CrossRef]
38. Marquardt, R. Modular Multilevel Converters: State of the Art and Future Progress. *IEEE Power Electron. Mag.* **2018**, *5*, 24–31. [CrossRef]
39. Chandio, R.H.; Chachar, F.A.; Soomro, J.B.; Ansari, J.A.; Munir, H.M.; Zawbaa, H.M.; Kamel, S. Control and Protection of MMC-Based HVDC Systems: A Review. *Energy Rep.* **2023**, *9*, 1571–1588. [CrossRef]
40. Raju, M.N.; Sreedevi, J.; Mandi, R.P.; Meera, K.S. Modular Multilevel Converters Technology: A Comprehensive Study on Its Topologies, Modelling, Control and Applications. *IET Power Electron.* **2019**, *12*, 149–169. [CrossRef]
41. Kutay, M.; Usman, A.M. A Survey on HVDC Power Transmission Systems. *Bilecik Seyh Edebali Univ. J. Sci.* **2020**, *7*, 1170–1181. [CrossRef]
42. Yu, J.; Karady, G.G.; Gu, L. Applications of Embedded HVDC in Power System Transmission. In Proceedings of the Power Engineering and Automation Conference, PEAM 2012, Wuhan, China, 18–20 September 2012. [CrossRef]
43. Zafari, L.; Liu, Y.; Ukil, A.; Nair, N.K.C. Advances in HVDC Systems: Aspects, Principles, and a Comprehensive Review of Signal Processing Techniques for Fault Detection. *Energies* **2025**, *18*, 3106. [CrossRef]
44. ENTSOE. *HVDC Links in System Operations*; ENTSOE: Bruxelles, Belgium, 2019.
45. Leterme, W.; Tielens, P.; De Boeck, S.; Van Hertem, D. Overview of Grounding and Configuration Options for Meshed HVDC Grids. *IEEE Trans. Power Deliv.* **2014**, *29*, 2467–2475. [CrossRef]
46. Ashouri, M.; Bak, C.L.; Faria Da Silva, F. A Review of the Protection Algorithms for Multi-Terminal VCD-HVDC Grids. In Proceedings of the IEEE International Conference on Industrial Technology 2018, Lyon, France, 20–22 February 2018; pp. 1673–1678. [CrossRef]
47. Muniappan, M. A Comprehensive Review of DC Fault Protection Methods in HVDC Transmission Systems. *Prot. Control Mod. Power Syst.* **2021**, *6*, 1–20. [CrossRef]
48. Psaras, V.; Emhemed, A.; Adam, G.; Burt, G. Review and Evaluation of the State of the Art of DC Fault Detection for HVDC Grids. In Proceedings of the 2018 53rd International Universities Power Engineering Conference, UPEC 2018, Glasgow, UK, 4–7 September 2018. [CrossRef]
49. Chen, Q.; Li, Q.; Wu, J.; He, J.; Mao, C.; Li, Z.; Yang, B. State Monitoring and Fault Diagnosis of HVDC System via KNN Algorithm with Knowledge Graph: A Practical China Power Grid Case. *Sustainability* **2023**, *15*, 3717. [CrossRef]
50. Candelaria, J.; Park, J. Do VSC-HVDC System Protection: A Review of Current Methods. In Proceedings of the 2011 IEEE/PES Power Systems Conference and Exposition, PSCE 2011, Phoenix, AZ, USA, 20–23 March 2011. [CrossRef]
51. Wang, G.; Xie, J.; Wang, S.; Jawad, R.S.; Abid, H. HVDC Fault Detection and Classification with Artificial Neural Network Based on ACO-DWT Method. *Energies* **2023**, *16*, 1064. [CrossRef]
52. Meghwani, A.; Srivastava, S.C.; Chakrabarti, S. A Non-Unit Protection Scheme for DC Microgrid Based on Local Measurements. *IEEE Trans. Power Deliv.* **2017**, *32*, 172–181. [CrossRef]
53. Pragati, A.; Mishra, M.; Rout, P.K.; Gadanayak, D.A.; Hasan, S.; Prusty, B.R. A Comprehensive Survey of HVDC Protection System: Fault Analysis, Methodology, Issues, Challenges, and Future Perspective. *Energies* **2023**, *16*, 4413. [CrossRef]
54. Rafferty, J.; Xu, L.; Morrow, D.J. DC Fault Analysis of VSC Based Multi-Terminal HVDC Systems. In Proceedings of the IET Conference Publications, Birmingham, UK, 4–5 December 2012. [CrossRef]
55. Liu, D.; Wei, T.; Huo, Q.; Wu, L. DC Side Line-to-Line Fault Analysis of VSC-HVDC and DC-Fault-Clearing Methods. In Proceedings of the 5th IEEE International Conference on Electric Utility Deregulation, Restructuring and Power Technologies, DRPT, Changsha, China, 26–29 November 2015; Volume 2016, pp. 2395–2399. [CrossRef]
56. Khaimar, A.K.; Shah, P.J. Study of Various Types of Faults in HVDC Transmission System. In Proceedings of the International Conference on Global Trends in Signal Processing, Information Computing and Communication, ICGTSPICC, Jalgaon, India, 22–24 December 2016; Volume 2017, pp. 480–484. [CrossRef]
57. Yang, J.; Fletcher, J.E.; O'Reilly, J. Short-Circuit and Ground Fault Analyses and Location in VSC-Based DC Network Cables. *IEEE Trans. Ind. Electron.* **2012**, *59*, 3827–3837. [CrossRef]
58. Zhao, P.; Chen, Q.; Xing, L. DC Fault Analysis of VSC-HVDC and DC Cable Protection Principle. In Proceedings of the Asia-Pacific Power and Energy Engineering Conference, APPEEC, Brisbane, Australia, 15–18 November 2015. [CrossRef]
59. Wang, Y.; Zhang, Z.; Fu, Y.; Hei, Y.; Zhang, X. Pole-to-Ground Fault Analysis in Transmission Line of DC Grids Based on VSC. In Proceedings of the 2016 IEEE 8th International Power Electronics and Motion Control Conference, IPEMC-ECCE Asia 2016, Hefei, China, 22–26 May 2016; pp. 2028–2032. [CrossRef]

60. Omorogbe, P.A.; Griffiths, A.; Ikhide, M.; Tennakoon, S. An Investigation of the Distinct Features of Wavelet Transform Based Protection Strategy for Consideration in HVDC Grids. In Proceedings of the 2021 IEEE Southern Power Electronics Conference, SPEC 2021, Kigali, Rwanda, 6–9 December 2021. [CrossRef]
61. Ha, H.; Subramanian, S. *Implementing the Protection and Control of Future DC Grids*; Academia: San Francisco, CA, USA, 2014.
62. Leterme, W.; Wang, M.; Van Hertem, D. Fault Discrimination in HVDC Grids with Reduced Use of HVDC Circuit Breakers. In Proceedings of the IEEE Power and Energy Society General Meeting 2018, Portland, OR, USA, 5–10 August 2018. [CrossRef]
63. Díaz, J.; Abarrategi, O.; Larruskain, D.M.; Perez-Basante, A.; Rubio, A. ROCOV Scheme for Fault Detection and Location in HVDC Sytems. *Renew. Energy Power Qual. J.* **2019**, *17*, 429–434. [CrossRef]
64. Lacerda, V.A.; Campos-Gaona, D.; Pena-Alzola, R.; Monaro, R.M.; Coury, D.V.; Anaya-Lara, O. Comparative Analysis of Fault Detection and Classification Techniques for HVDC Grids Protection. In Proceedings of the 15th International Conference on Developments in Power System Protection (DPSP 2020), Liverpool, UK, 9–12 March 2020. [CrossRef]
65. Raghpoor, V.; Mehrabi-Kooshki, M.; Razzaghi, R. A Novel Non-Unit Protection Scheme for HVDC Transmission Lines Based on Multi-Resolution Morphology Gradient. *IET Gener. Transm. Distrib.* **2021**, *15*, 894–911. [CrossRef]
66. Perez-Molina, M.J.; Larruskain, D.M.; Eguia Lopez, P.; Buigues, G.; Valverde, V. Review of Protection Systems for Multi-Terminal High Voltage Direct Current Grids. *Renew. Sustain. Energy Rev.* **2021**, *144*, 111037. [CrossRef]
67. Ikhide, M.; Tennakoon, S.B.; Ha, H.; Griffiths, A.L.; Subramanian, S.; Adamczyk, A.J. A Transient and Non-Unit-Based Protection Technique for DC Grids Based on the Rate-of-Change (R-o-C) of the Fault Induced Travelling Wave Components. *Sustain. Energy Grids Netw.* **2019**, *17*, 100195. [CrossRef]
68. Pazoki, M.; Yadav, A.; Abdelaziz, A.Y. Pattern-Recognition Methods for Decision-Making in Protection of Transmission Lines. In *Decision Making Applications in Modern Power Systems*; Academic Press: Cambridge, MA, USA, 2019; pp. 441–472. [CrossRef]
69. Li, D.; Ukil, A. Empirical Mode Decomposition Based DC Fault Detection Method in Multi-Terminal DC System. In Proceedings of the IEEE Power and Energy Society General, Montreal, QC, Canada, 2–6 August 2020. [CrossRef]
70. Gnanamalar, A.J.; Bhavani, R.; Arulini, A.S.; Veerraju, M.S. CNN–SVM Based Fault Detection, Classification and Location of Multi-Terminal VSC–HVDC System. *J. Electr. Eng. Technol.* **2023**, *18*, 3335–3347. [CrossRef]
71. Ashouri, M.; Faria da Silva, F.; Leth Bak, C. Analysis and Validation of Mathematical Morphology Filters for Single-Ended Fault Localization in VSC-HVDC Links. *Electr. Eng.* **2021**, *103*, 1583–1596. [CrossRef]
72. Aleem, S.A.; Shahid, N.; Naqvi, I.H. Methodologies in Power Systems Fault Detection and Diagnosis. *Energy Syst.* **2014**, *6*, 85–108. [CrossRef]
73. Kaur, J.; Jayasooriya, M.; Iqbal, M.N.; Daniel, K.; Shabbir, N.; Peterson, K. Fault Detection and Protection Strategy for Multi-Terminal HVDC Grids Using Wavelet Analysis. *Energies* **2025**, *18*, 1147. [CrossRef]
74. Saleem, U.; Arshad, U.; Masood, B.; Gul, T.; Khan, W.A.; Ellahi, M. Faults Detection and Classification of HVDC Transmission Lines of Using Discrete Wavelet Transform. In Proceedings of the 2018 International Conference on Engineering and Emerging Technologies, ICEET 2018, Lahore, Pakistan, 22–23 February 2018; pp. 1–6. [CrossRef]
75. Lacerda, V.A.; Monaro, R.M.; Campos-Gaona, D.; Coury, D.V.; Anaya-Lara, O. Distance Protection Algorithm for Multiterminal HVDC Systems Using the Hilbert–Huang Transform. *IET Gener. Transm. Distrib.* **2020**, *14*, 3022–3032. [CrossRef]
76. Narayana, S.; Ramesh, B.; Hussain, S. Identification of Faults in HVDC System Using Wavelet Analysis. *Int. J. Electr. Comput. Eng.* **2011**, *2*, 175–182. [CrossRef]
77. Paily, B. HVDC Systems Fault Analysis Using Various Signal Processing Techniques. Ph.D. Thesis, Technological University Dublin, Dublin, Ireland, 2015. [CrossRef]
78. Sahebkar Farkhani, J.; Çelik, Ö.; Ma, K.; Bak, C.L.; Chen, Z. A Comprehensive Review of Potential Protection Methods for VSC Multi-Terminal HVDC Systems. *Renew. Sustain. Energy Rev.* **2024**, *192*, 114280. [CrossRef]
79. De Kerf, K.; Srivastava, K.; Reza, M.; Bekaert, D.; Cole, S.; Van Hertem, D.; Belmans, R. Wavelet-Based Protection Strategy for DC Faults in Multi-Terminal VSC HVDC Systems. *IET Gener. Transm. Distrib.* **2011**, *5*, 496–503. [CrossRef]
80. Pinsky, M. *Introduction to Fourier Analysis and Wavelets*; American Mathematical Society (AMS): Providence, RI, USA, 2023.
81. Mallat, S.G. A Theory for Multiresolution Signal Decomposition: The Wavelet Representation. *IEEE Trans. Pattern Anal. Mach. Intell.* **1989**, *11*, 674–693. [CrossRef]
82. Littler, T.B.; Morrow, D.J. Wavelets for the Analysis and Compression of Power System Disturbances. *IEEE Trans. Power Deliv.* **1999**, *14*, 358–364. [CrossRef]
83. Pothisarn, C.; Klomjit, J.; Ngaopitakkul, A.; Jettanasen, C.; Asfani, D.A.; Negara, I.M.Y. Comparison of Various Mother Wavelets for Fault Classification in Electrical Systems. *Appl. Sci.* **2020**, *10*, 1203. [CrossRef]
84. Yeap, Y.M.; Geddada, N.; Ukil, A. Analysis and Validation of Wavelet Transform Based DC Fault Detection in HVDC System. *Appl. Soft Comput.* **2017**, *61*, 17–29. [CrossRef]
85. Wang, Y.; Ren, Z.; Li, Q. Wavelets Selection for Commutation Failure Detection in HVDC System. In Proceedings of the IEEE Region 10 Annual International Conference, Proceedings/TENCON, Hong Kong, China, 14–17 November 2007. [CrossRef]

86. Budak, S.; Akbal, B. Estimation of High Impedance Fault Location in Electrical Transmission Lines Using Artificial Neural Networks and R-X Impedance Graph. *arXiv* **2020**, arXiv:2011.03227. [CrossRef]
87. Taheri, B.; Hosseini, S.A.; Sedighizadeh, M. Novel Hybrid Fuzzy-SVR Model for Fault Detection in VSC-HVDC Transmission Lines. *Int. J. Electr. Power Energy Syst.* **2025**, *172*, 111222. [CrossRef]
88. Yan, J.; Song, G.; Chang, Z.; Gao, X.; Zhang, C. Fault Location Method for MMC-HVDC Systems Based on Numerical Laplace Transform. *IEEE Trans. Power Deliv.* **2024**, *39*, 2603–2615. [CrossRef]
89. Raza, A.; Hamza, M.A.; Kashif, A.R.; Yousaf, M.Z.; Khan, B.; Guerrero, J.M.; Sivanraju, R. Adaptive Non Unit Traveling Wave Protection Algorithm for Multi Terminal HVDC Grids. *Sci. Rep.* **2025**, *15*, 35536. [CrossRef]
90. Zhang, Y.; Yu, Y.; Yang, G. An Ultra-Fast MMC-HVDC Fault Location Algorithm Based on Transient Voltage Features and Regression Neural Network. *Int. J. Electr. Power Energy Syst.* **2024**, *162*, 110249. [CrossRef]